# Advances in computational methods for Quantum Field Theory calculations

Ruijl, B.J.G.

# 6 THE FIVE-LOOP BETA FUNCTION

In this chapter we report on the first computation of the five loop beta function for a general Yang-Mills theory with one set of fermions. This is only possible by combining the results of **RQ2**, the FORCER program for four-loop calculations described in chapter 3, and **RQ3**, the $R^*$-operation described in chapter 5.

The beta function governs how the strength of the strong interaction scales with the energy. The determination of the (sign of the) leading one-loop coefficient $\beta_0$ [23, 24], soon followed by the calculation of the two-loop correction $\beta_1$ [119, 210] shows that the strong interaction vanishes at large energies (or very short distances). This *asymptotic freedom* means that QCD is a viable theory for the strong interaction. The discovery of asymptotic freedom was awarded the Nobel Prize for Physics in 2004.

The scale dependence ('running') of the renormalised coupling constant $\alpha_i$ can be written in perturbation theory as

$$\frac{da}{d\ln\mu^2} = \beta(a) = -\sum_{n=0}^{\infty} \beta_n a^{n+2}, \quad a = \frac{\alpha_i(\mu)}{4\pi} \tag{240}$$

where $\mu$ is the renormalisation scale.

The renormalisation-scheme dependent three-loop (next-to-next-to-leading order, N$^2$LO) and four-loop (next-to-next-to-next-to-leading order, N$^3$LO) coefficients $\beta_2$ and $\beta_3$ were computed in refs. [122, 211] and [113, 114] in minimal subtraction schemes [130, 131] of dimensional regularisation [179, 180].

Precise determination of the beta function is important for all renormalisation group improved perturbation theory calculations. Below we mention two important use-cases. First, in the past years, N$^2$LO accuracy has been reached for many processes at high-energy colliders. N$^3$LO corrections have been determined for structure functions in inclusive deep-inelastic scattering (DIS) [98, 212] and for the total cross section for Higgs-boson production at hadron colliders [82, 155]. Second, we have computed moments of coefficient functions for DIS at N$^4$LO [8]. Obtaining full results at this order would virtually remove the uncertainty due to the truncation of the series of massless perturbative QCD in determinations of the strong coupling constant $\alpha_s$ from the scaling violations of structure functions in DIS.

The corresponding five-loop contributions to the beta functions of QCD, with all colour factors 'hard-wired', and QED have already been computed in refs. [40, 213]. Their leading large-$n_f$ contributions have long been known [214], and the sub-leading large-$n_f$ terms have been checked and generalized to a general simple gauge group in ref. [128]. The real tour de force of ref. [40] though, are the parts proportional to $n_f^0$, $n_f^1$ and $n_f^2$ which together required more than a year of computations on 20 multi-core workstations in a highly non-trivial theoretical framework. These critical

parts have neither been extended to a general gauge group nor validated by a second independent calculation.

In the following chapter we address this issue and present the five-loop beta function for a general simple compact gauge group. Unlike the calculations in refs. [23, 24, 113, 114, 119, 120, 122, 210, 211], we have employed the background field method (see section 6.2), and the $R^*$ method (see chapter 5).

Finally, we transform the five-loop Yang-Mills beta function from $\overline{\text{MS}}$ to the MiniMOM scheme [153]. The MiniMOM scheme is more convenient than $\overline{\text{MS}}$ for analysis in the non-perturbative regime of QCD.

The remainder of this chapter is structured as follows. We first explore five optimisations in section 6.1, after which we define the background field in section 6.2. Next, we present the computation of the five-loop beta function for Yang-Mills theory with fermions in section 6.3. We discuss the results in section 6.4. In section 6.5, we transform the five-loop beta function from $\overline{\text{MS}}$ to the MiniMOM scheme. Finally, we present the chapter conclusions in section 6.6.

## 6.1 OPTIMISATIONS

Performing computations at five loops introduces at least five new bottlenecks compared to four loops. (1) The number of diagrams and their complexity grow exponentially. (2) The substitution of the Feynman rules is slow and creates millions of term. (3) The Taylor expansion to make the diagrams logarithmic creates many terms. (4) The number of counterterms grows exponentially. (5) Tensors of rank 10 have to be reduced, which involves solving large systems.

In this section we address these issues by presenting five optimisations, namely improved treatment of propagator insertions in section 6.1.1, delayed Feynman rule substitution in section 6.1.2, improved rules to make diagrams logarithmic in section 6.1.3, a canonical form algorithm for Feynman diagrams in section 6.1.4, and an efficient tensor reduction algorithm in section 6.1.5.

### 6.1.1 *Treatment of propagator insertions*

Many of the higher-loop corrections are self-energies of propagators in the diagram. Due to the local nature of the Feynman rules, these self-energies only depend on

their external momentum (there are no contractions with other parts of the larger diagram), so they can be 'factorised' out (see also 3.10):

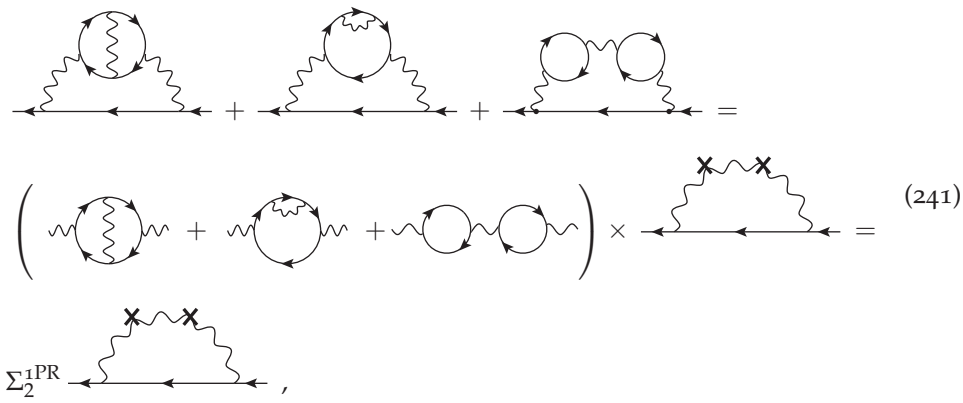

(241)

where the $L$-loop self-energy is replaced by $(p^2)^{-\varepsilon L}$ in the larger diagram (marked by $L$ crosses). In a sense, the subdiagram is integrated out. The resulting simpler topology is multiplied by the one-particle-reducible $L$-loop self-energy. Since the $L$-loop subdiagram is of lower order, these quantities have already been computed and can easily be tabulated to prevent recomputations. For example, a five-loop diagram may contain the expensive 4-loop gluon propagator as a subdiagram.

For the $R^*$-operation, this representation has an issue: the non-integer power hides UV-divergent subdiagrams, which should be subtracted. However, since the exact contents of the $(p^2)^{-\varepsilon L}$ is factorised out, we may replace it with *any* $L$-loop subdiagram. Therefore we choose the simplest configuration: $L$ scalar one-loop bubbles side by side.

Thus, for the $R^*$-operation we can remove propagator insertions by using the following relation:

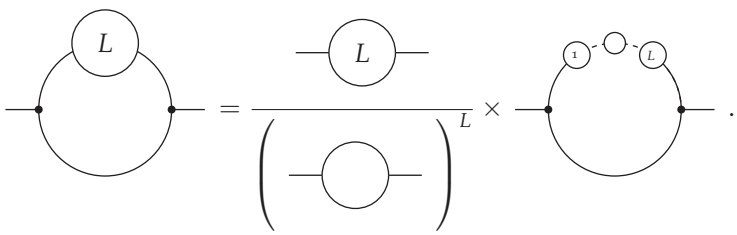

(242)

### 6.1.2 *Delayed Feynman rule substitution*

Substituting the Feynman rules creates many terms. For example, the following fully gluonic five-loop graph creates 12 029 521 scalar integrals in the Feynman gauge:

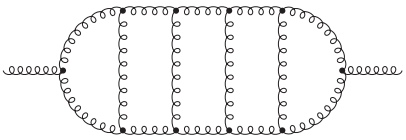

(243)

The source of the blow-up is the Feynman rule for the triple gluon vertex, which can be written in the following way:

$$v_{3g}(p_1^{\mu,a}, p_2^{\nu,b}, p_3^{\rho,c}) = -if^{abc}\left[(p_1-p_2)^\rho g_{\mu\nu} + (2p_2+p_1)^\mu g_{\nu\rho} + (-2p_1-p_2)^\nu g_{\mu\rho}\right] . \tag{244}$$

Thus, for every vertex, six terms are created, of which some will evaluate to the same expression due to symmetries. For all these terms, expensive operations such as Taylor expansions and divergent subgraph recognitions have to be performed. However, these operations only depend on the momentum powers and are invariant under the way the momenta contract. So, we rewrite the triple gluon vertex in a way that exposes the momenta, but keeps all the contractions unsubstituted:

$$v_{3g}(p_1^{\mu,a}, p_2^{\nu,b}, p_3^{\rho,c}) = -if^{abc}p_1^\sigma t_3(\sigma,\nu,\rho,\mu) + if^{abc}p_2^\sigma t_3(\sigma,\mu,\rho,\nu) , \tag{245}$$

where

$$t_3(\mu,\nu,\rho,\sigma) = g_{\mu\rho}g_{\nu\sigma} + g_{\mu\sigma}g_{\nu\rho} - 2g_{\mu\nu}g_{\rho\sigma} . \tag{246}$$

After rewriting $v_{3g}$ in terms of $t_3$, there are only $2^{10} = 1024$ terms for the Feynman diagram in eq. (243). We can keep our input in this compactified notation for as long as the actual contractions are not important, which is right until the tensor reduction.

We define the operation $\circ$ that applies the remaining Feynman rules to all components of the $R^*$-operation. For example:

$t_3(\mu,\nu,\rho,\sigma) \circ \Delta$ 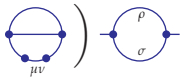 $= 2\Delta$ 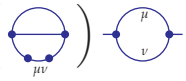 $- 2\Delta$ 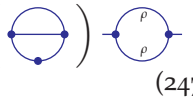 . (247)

We stress that for this particular case contraction is *necessary*.

Similar rules can be devised for the other vertices and for the trace of gamma matrices. At five loops, the substitution of $t_3$ and similar structures is an expensive part of the calculation, since the number of generated terms is high.

### 6.1.3 *Rules to make Feynman diagrams logarithmic*

Since we compute

$$K(G) = -K\delta R^* G , \tag{248}$$

we can make $G$ logarithmic, by d'Alembertian-like derivatives inside $K(G)$. The advantage over just Taylor expanding $\Delta(G)$, is that we are allowed to contract inside $K(G)$. We first consider the following linear integral $F$:

$$F = Q^\mu F^\mu, \qquad F^\mu = Q^\mu (Q^2)^{-\epsilon L} f(\epsilon) \; . \tag{249}$$

We take the following derivative and solve the new equation for $F$:

$$\begin{aligned} \partial_\mu F^\mu &= (1-2\epsilon L)(Q^2)^{-\epsilon L} f(\epsilon) \\ f(\epsilon) &= \frac{1}{1-2\epsilon L}(Q^2)^{\epsilon L}\partial_\mu F^\mu \\ F &= \frac{Q^2}{1-2\epsilon L}\partial_\mu F^\mu \; . \end{aligned} \tag{250}$$

Thus, we have re-expressed $F$ into a logarithmic integral with a new dot product that is internal to the graph. For the $R^*$-operation, this is generally better than a dot product with $Q$, since a dot product with the external momentum always requires a projection whereas internal momenta may be in the same divergent subdiagram.

For quadratic integrals $F$, we can apply the d'Alembertian to achieve the same effect:

$$\begin{aligned} F &= (Q^2)^{1-\epsilon L} f(\epsilon) \\ \Box F &= 4(\epsilon L - 1)(\epsilon(L+1)-2)(Q^2)^{1-\epsilon L} f(\epsilon) \\ F &= \frac{Q^2}{4(\epsilon L-1)(\epsilon(L+1)-2)}\Box F \; . \end{aligned} \tag{251}$$

For quadratic integrals of the form $Q^\mu Q^\nu F^{\mu\nu}$, we can derive a special rule as well:

$$F = \frac{\partial_\mu \partial_\nu F^{\mu\nu}(2-2\epsilon L) + \partial_\alpha \partial^\alpha F^{\mu\mu}}{-8(-1+\epsilon L)(-3+\epsilon+\epsilon L)(-2+\epsilon+\epsilon L)} \tag{252}$$

For integrals with more $Q$s, or higher than quadratic ones, there are not sufficient ways available to contract existing vectors to solve the system. To make these integrals logarithmic, one could use Euler's homogeneous function theorem:

$$Q^\alpha \partial_\alpha F = nF \; , \tag{253}$$

where $n$ is the order in $Q$. For a Feynman integral of degree $S$ we have $n = S - 2\epsilon L$. Thus we formulate:

$$F = \left(\frac{1}{S-2\epsilon L} Q^\alpha \partial_\alpha\right)^S F \tag{254}$$

Every time a derivative is taken, another $Q$-path can be chosen through the diagram, to limit the growth of the number of terms. However, since the shape of eq. (254) is similar to a Taylor expansion, it is faster to only perform the Taylor expansion on $\Delta(G)$.

It is important to construct the counterterms of the rearranged $G'$ at the same time as the subdivergences of $G$. Since many counterterms of $G$ are also in $G'$, the number of relevant counterterms is reduced. This saves a factor three at four loops.

### 6.1.4 *Canonical forms for Feynman diagrams*

The $R^*$-operation applied to five-loop diagrams will create many counterterms. In order to reduce computation time, it is important to compute the counterterms of a specific graph only once. In turn, this requires an efficient way to detect if two graphs are equal. One straightforward option is to keep a list of all the graphs that have already been processed and test for isomorphisms on every element of the list until one is found. If no match is found, the current graph can be added to the list. The two downsides of this method are that (1) an isomorphism test can be rather slow at five loops and (2) that the list of topologies grows rapidly.

A better alternative is to construct a *canonical form* of a graph. A canonical form is an isomorphism of the graph that is designated as the smallest by some yet to be defined measure. To test for equality, one can simply compare the canonical forms. Since isomorphy is first and foremost a property of the vertices, we give each vertex a label from 1 to $n$. For simplicity, let us consider a graph that has no dot products and only has edges with power 1.

We convert our graph to an edge representation:

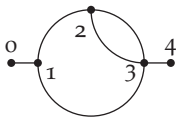


$$= e(0,1)e(1,2)e(2,3)e(2,3)e(1,3)e(3,4)\ . \tag{255}$$

Here, $e(n_1, n_2)$ is the edge function, in which we place the smallest vertex index as the first argument. The *edge list* is a lexicographically sorted list of edge functions, as is shown in eq. (255). Now we define the smallest isomorphism of a graph as the vertex labelling for which the edge list is lexicographically smallest.[1]

We can easily extend the graph notation to a graph where propagators can have different powers, by introducing a third argument to the edge function $e$:

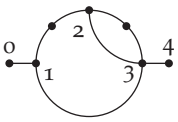


$$= e(0,1,1)e(1,2,2)e(2,3,1)e(2,3,2)e(1,3,1)e(3,4,1)\ , \tag{256}$$

where we again make sure that the first two arguments of $e(n_1, n_2, \ldots)$ are sorted. To add support for dot products and tensors, we extend the edge function even further:

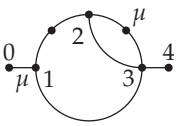


$$= e(0,1,1,\mu)e(1,2,2)e(2,3,1)e(2,3,2,\mu)e(1,3,1)e(3,4,1)\ . \tag{257}$$

1 In our program, we use the internal (deterministic) sorting order of Form to determine the smallest isomorphism instead.

We define the canonical signs of the momenta such that they always flow from the smallest vertex label to the highest. If a transformation changes the order, we flip the sign if the number of vectors in the momentum is odd:

$$e(2,1,n,\mu_1,\ldots,\mu_k) = (-1)^k e(1,2,n,\mu_1,\ldots,\mu_k)\,. \tag{258}$$

Finally, the momentum label $p_i$ of each edge is uniquely defined by the position $i$ of the edge in the edge list.

Now that most properties of the Feynman integral are captured in the extended edge list and we have defined which edge list is smallest, we use McKay's canonicalisation algorithm [215] to efficiently rewrite the complete Feynman integral to canonical form. A simplified version of this algorithm is implemented in Form code.

### 6.1.5 *Efficient tensor reduction*

It can be shown that the tensor reduction of ultraviolet and infrared subtraction terms, required for the $R^*$-operation, is equivalent to the tensor reduction of tensor vacuum bubble integrals. In general tensor vacuum integrals can be reduced to linear combinations of products of metric tensors $g^{\mu\nu}$ whose coefficients are scalar vacuum integrals. Specifically a rank $r$ tensor, $T^{\mu_1\cdots\mu_r}$, is written as a linear combination of $n = r!/2^{(r/2)}/(r/2)!$ combinations of $(r/2)$ metric tensors with coefficients $c_\sigma$, i.e.,

$$T^{\mu_1\cdots\mu_r} = \sum_{\sigma\in{}_2S_r} c_\sigma\, T_\sigma^{\mu_1\cdots\mu_r}\,, \qquad T_\sigma^{\mu_1\cdots\mu_r} = g^{\mu_{\sigma(1)}\mu_{\sigma(2)}}\cdots g^{\mu_{\sigma(r-1)}\mu_{\sigma(r)}}\,. \tag{259}$$

Here we define ${}_2S_r$ as the group of permutations which do *not* leave the tensor $T_\sigma^{\mu_1\cdots\mu_r}$ invariant. The coefficients $c_\sigma$ can be obtained by acting onto the tensor $T^{\mu_1\cdots\mu_r}$ with certain projectors $P_\sigma^{\mu_1\cdots\mu_r}$, such that

$$c_\sigma = P_\sigma^{\mu_1\cdots\mu_r} T_{\mu_1\ldots\mu_r}\,. \tag{260}$$

From this it follows that the orthogonality relation,

$$P_\sigma^{\mu_1\cdots\mu_r} T_{\tau,\mu_1\ldots\mu_r} = \delta_{\sigma\tau}\,, \tag{261}$$

must hold, where $\delta$ is the Kronecker-delta. Since the projector $P_\sigma^{\mu_1\cdots\mu_r}$ of each tensor can also be written in terms of a linear combination of products of metric tensors, inverting an $n\times n$ matrix determines all the projectors. However, there are two issues. The first is that the size of the matrix grows rather rapidly as $r$ increases. Instead of solving an $n\times n$ linear system, the symmetry group of the metric tensors can be utilised to reduce the size of the system. From eq. (261) it follows that the projector $P_\sigma$ is in the same symmetry group (the group of permutations which leave it invariant) as $T_\sigma$. For example, given a permutation $\sigma_1 = (123...(r-1)r)$,

$$T_{\sigma_1}^{\mu_1\cdots\mu_r} = g^{\mu_1\mu_2} g^{\mu_3\mu_4}\cdots g^{\mu_{r-1}\mu_r}\,. \tag{262}$$

The corresponding projector $P_{\sigma_1}^{\mu_1\cdots\mu_r}$ must be symmetric under interchanges of indices such as $\mu_1\leftrightarrow\mu_2$, $(\mu_1,\mu_2)\leftrightarrow(\mu_3,\mu_4)$ and so on. Grouping the metric tensors by the

symmetry leads to the fact that $P_\sigma$ is actually written in a linear combination of a small number of $m$ tensors instead of $n$ ($m \leq n$),

$$P_\sigma^{\mu_1 \cdots \mu_r} = \sum_{k=1}^{m} b_k \sum_{\tau \in A_m^\sigma} T_\tau^{\mu_1 \cdots \mu_r}. \tag{263}$$

The set of groups $\{A_k^\sigma | k = 1..m\}$ must therefore each be closed under the permutations which leaves $T_\sigma$ invariant and at the same time their union must cover once the group ${}_2S_n$. Contracting $P_\sigma$ with a representative in each group gives an $m \times m$ matrix which can be inverted to yield the coefficients $b_k$. The number of unknowns $m$ is $m = 5$ for $r = 8$ and $m = 22$ for $r = 16$, whereas we have $n = 105$ for $r = 8$ and $n = 2027025$ for $r = 16$. The comparison of these numbers illustrates that the exploitation of the symmetry of the projectors makes it possible to find the tensor reduction even for very large values of $r$, which could never have been obtained by solving the $n \times n$ matrix.

The second issue with tensors of high rank is the large number of intermediate terms that are created. Even though the system for the projector can be solved efficiently, $\mathcal{O}(n^2)$ terms will be created, of which some will merge due to symmetry. Let us consider rank 6, with 15 terms:

$$c_1 g^{\mu_1\mu_2} g^{\mu_3\mu_4} g^{\mu_5\mu_6} + c_2 g^{\mu_1\mu_3} g^{\mu_2\mu_4} g^{\mu_5\mu_6} + \dots . \tag{264}$$

In most practical situations there is symmetry, both on the inside of the object that will be projected as on the outside. For example

$$A(p_1^{\mu_1} p_1^{\mu_2} p_1^{\mu_3} p_1^{\mu_4} p_2^{\mu_5} p_2^{\mu_6}) p_3^{\mu_1} p_3^{\mu_2} p_4^{\mu_3} p_4^{\mu_4} p_4^{\mu_5} p_4^{\mu_6} \tag{265}$$

is symmetric in exchanges of $\mu_1, \dots, \mu_4$ and $\mu_5, \mu_6$ inside $A$, and is symmetric in $\mu_1, \mu_2$ and $\mu_3, \dots, \mu_6$ outside $A$. The symmetry inside the object $A$ will enforce that coefficient $c_1$ and $c_2$ (and others) will actually be the same. The symmetry on the outside will cause terms to merge. In the end, we could have used the symmetrised variant of eq. (264) instead:

$$c_1 \cdot (g^{\mu_1\mu_2} g^{\mu_3\mu_4} g^{\mu_5\mu_6} + 2 g^{\mu_1\mu_3} g^{\mu_2\mu_4} g^{\mu_5\mu_6}) + c_3 (2 g^{\mu_1\mu_2} g^{\mu_3\mu_5} g^{\mu_4\mu_6} + 10 g^{\mu_1\mu_5} g^{\mu_2\mu_6} g^{\mu_3\mu_4}). \tag{266}$$

We see that only two coefficients have to be computed instead of 15 and that there are only 4 terms in the output instead of 15. The challenge is to prevent these terms from being created in the first place by exploiting symmetry, instead of starting from eq. (264). We make use of the optimised Form command `dd_`, which creates the tensor structure $T^{\mu_1,\dots,\mu_r}$ without generating duplicates. If we evaluate `dd_(p1,p1,p1,p1,p2,p2)` and strip the coefficient we get `p1.p1^2*p2.p2+p1.p1*p1.p2^2`. These two terms represent the structure outside of $c_1$ and $c_3$ in (266). For each of these two terms, we solve for the coefficient. Next, we recreate the metric structures that would give this specific contraction.

A term generated by `dd_` consists of two different factors: $(p \cdot p)^a$ and $(p_1 \cdot p_2)^a$. For $(p \cdot p)^a$, we collect all possible indices involved with $p$. For eq. (265), this would

be $\mu_1, \ldots, \mu_4$. Then we select all possible ways to get $2a$ elements from that list with `distrib_`. Next, we use $dd_-$ on those indices. Thus, for $p_1 \cdot p_1$ in the example we would get $g^{\mu_1\mu_2} + g^{\mu_1\mu_3} + g^{\mu_2\mu_3}$. For cases such as $(p_1 \cdot p_2)^a$, we select $a$ from the list of indices associated to $p_1$ and $a$ from the list of $p_2$. Then we permute over the list of $p_2$. Using this algorithm, one can generate all possible contractions from the result without generating duplicates. To apply the outside symmetry, one can easily fill in the outside momenta associated to the indices instead of the indices themselves. `distrib_` and `dd_` will take the symmetry into account automatically.

## 6.2 THE BACKGROUND FIELD

A convenient and efficient method to extract the Yang-Mills beta function is to make use of the background field. We will briefly review this formalism. We start with the Lagrangian of Yang-Mills theory coupled to fermions in a non-trivial (often the fundamental) representation of the gauge group, the theory for which we will present the five-loop beta-function in section 6.3.

The Lagrangian of this theory can be decomposed as

$$\mathcal{L}_{\text{YM+FER}} = \mathcal{L}_{\text{CYM}} + \mathcal{L}_{\text{GF}} + \mathcal{L}_{\text{FPG}} + \mathcal{L}_{\text{FER}} \,. \tag{267}$$

Here the classical Yang-Mills Lagrangian (CYM), a gauge-fixing term (GF), the Faddeev-Popov ghost term (FPG) and the fermion term (FER) are given by

$$\begin{aligned}
\mathcal{L}_{\text{CYM}} &= -\frac{1}{4} F^a_{\mu\nu}(A) F^{\mu\nu}_a(A) \,, \\
\mathcal{L}_{\text{GF}} &= -\frac{1}{2\xi} (G^a)^2 \,, \\
\mathcal{L}_{\text{FPG}} &= -\eta^\dagger_a \, \partial^\mu D^{ab}_\mu(A) \, \eta_b \,, \\
\mathcal{L}_{\text{FER}} &= \sum_{i,j,f} \bar{\psi}_{if} (i \not{D}_{ij}(A) - m_f \delta_{ij}) \, \psi_{jf} \,.
\end{aligned} \tag{268}$$

In the fermion term the sum goes over colours $i, j$, and $n_f$ flavours $f$, and we use the standard Feynman-slash notation. The field strength is given by

$$F^a_{\mu\nu}(A) = \partial_\mu A^a_\nu - \partial_\nu A^a_\mu + g f^{abc} A^b_\mu A^c_\nu \tag{269}$$

and the covariant derivatives are defined as

$$\begin{aligned}
D^{ab}_\mu(A) &= \delta^{ab} \partial_\mu - g f^{abc} A^c_\mu \,, \\
D^\mu_{ij}(A) &= \delta_{ij} \partial^\mu - i g \, T^a_{ij} A^\mu_a \,.
\end{aligned} \tag{270}$$

The conventions associated to the generators $T^a$ and structure constants $f^{abc}$ of the gauge group will be explained in section 4.1. The gauge-fixing term depends on making a suitable choice for $G^a$, which is usually taken as $G^a = \partial^\mu A^a_\mu$.

The background-field Lagrangian is derived by decomposing the gauge field as

$$A^a_\mu(x) \;=\; B^a_\mu(x) + \hat{A}^a_\mu(x)\,, \tag{271}$$

where $B^a_\mu(x)$ is the *classical* background field while $\hat{A}^a_\mu(x)$ contains the *quantum* degrees of freedom of the gauge field $A^a_\mu(x)$. The background-field Lagrangian is then written as

$$\mathcal{L}_{\text{BYM+FER}} \;=\; \mathcal{L}_{\text{BCYM}} + \mathcal{L}_{\text{BGF}} + \mathcal{L}_{\text{BFPG}} + \mathcal{L}_{\text{BFER}}\,. \tag{272}$$

$\mathcal{L}_{\text{BCYM}}$ and $\mathcal{L}_{\text{BFER}}$ are derived simply by substituting eq. (271) into the corresponding terms in the Yang-Mills Lagrangian. However a clever choice exists [117, 118] for the ghost and gauge fixing terms, which allows this Lagrangian to maintain explicit gauge invariance for the background field $B^a_\mu(x)$, while fixing only the gauge freedom of the quantum field $\hat{A}^a_\mu(x)$. The gauge fixing then uses instead

$$G^a \;=\; D^{ab}_\mu(B)\hat{A}^\mu_b\,, \tag{273}$$

while the ghost term is given by

$$\mathcal{L}_{\text{BFPG}} \;=\; -\eta^\dagger_a\, D^{ab;\mu}(B)\, D^{bc}_\mu(B+\hat{A})\,\eta_c\,. \tag{274}$$

The Lagrangian $\mathcal{L}_{\text{BYM+FER}}$ then gives rise to additional interactions which are different from the normal QCD interactions of the quantum field $\hat{A}^a_\mu(x)$ also contain interactions of $B^a_\mu(x)$ with all other fields.

A remarkable fact is found when considering the renormalisation of this Lagrangian. Indeed it turns out, see e.g., [117, 118], that the coupling renormalisation, $g \to Z_g\, g$, which determines the beta function, is directly related to the renormalisation of the background field, $B \to BZ_B$, via the identity:

$$Z_g\sqrt{Z_B} \;=\; 1\,. \tag{275}$$

When working in the Landau gauge, the only anomalous dimension needed in the background field gauge formalism is then the beta function. However in the Feynman gauge the gauge parameter $\xi$ requires the renormalisation constant $Z_\xi$ – which equals the gluon field renormalisation constant – but only to one loop lower. In turn this allows one to extract the beta function from the single equation

$$Z_B(1+\Pi_B(Q^2; Z_\xi\xi, Z_g g)) \;=\; \text{finite}, \tag{276}$$

with

$$\Pi^{\mu\nu}_B(Q; Z_\xi\xi, Z_g g) \;=\; (Q^2 g^{\mu\nu} - Q^\mu Q^\nu)\,\Pi_B(Q^2; Z_\xi\xi, Z_g g)\,, \tag{277}$$

where $\Pi^{\mu\nu}_B(Q^2;\xi,g)$ is the bare self energy of the background field. This self-energy is computed by keeping the fields $B$ external while the only propagating fields are $\hat{A}, \eta$ and $\psi$.

Obtaining the beta function through the background field gauge is faster and simpler than the traditional method of computing the gluon propagator, ghost propagator and ghost-ghost-gluon vertex due to a lower total number of diagrams and the above reduction to a scalar renormalisation. The number of diagrams for the background field propagator at four loops is 7435, whereas the smallest combination needed for the beta function (gluon and ghost propagator + ghost-ghost-gluon vertex) requires $5245 + 1507 + 18034 = 24786$ diagrams. This speed-up is also evident from figure 24, which shows that calculating the background field propagator takes about as much time as computing the gluon propagator.

The additional Feynman rules required for the background field propagator are displayed in table 5. The vertices with two background fields attached to it yield 0, since these are tadpoles.

Now that we have discussed several optimisations and defined the background field propagator, we can focus on the computation of the five-loop beta function.

## 6.3 DIAGRAM COMPUTATIONS AND ANALYSIS

As outlined in 6.2, it is possible to extract the five-loop beta function from the poles (in the dimensional regulator $\epsilon$) of the bare background field self-energy $\Pi_B(Q)$. It is beyond current computational capabilities to calculate the required five-loop propagator integrals directly. The main obstacle preventing such an attempt is the difficulty of performing the required IBP reductions (see section 3.5).

However, the problem can be simplified via the use of the $R^*$-operation. This allows us to decompose the five-loop integral into a five-loop counterterm and counterterms of lower loops. We infrared-rearrange (IRR) the five-loop counter term to a carpet integral. For example:

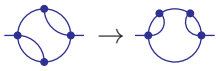 (278)

These carpet integrals can always be reduced to four loops (see section 3.3). If the counterterm is not logarithmic, we first apply the rules provided in section 6.1.3. After we use the FORCER program to compute the four-loop integrals.

The Feynman diagrams for the background propagator up to five loops have been generated using QGRAF [111]. They have then been heavily manipulated by a FORM [101, 102, 216] program that determines the topology and calculates the colour factor using the program of ref. [112]. Additionally, it merges diagrams of the same topology, colour factor, and maximal power of $n_f$ into meta diagrams for computational efficiency. Integrals containing massless tadpoles or symmetric colour tensors with an odd number of indices have been filtered out from the beginning. Lower-order self-energy insertions have been 'factorised' out. In this manner we arrive at 2 one-loop, 9 two-loop, 55 three-loop, 572 four-loop and 9414 five-loop meta diagrams. We refer the reader to section 3.10 for a more detailed description.

The diagrams up to four loops have been computed earlier to all powers of the gauge parameter using the FORCER program [1, 7, 9]. For the time being, our five-loop

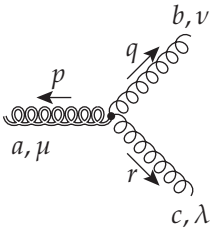


$$gf_{abc}\left[g_{\mu\lambda}\left(p-r-\frac{q}{\xi}\right)_{\nu}+g_{\nu\lambda}\left(r-q\right)_{\mu}+g_{\mu\nu}\left(q-p+\frac{r}{\xi}\right)_{\lambda}\right]$$

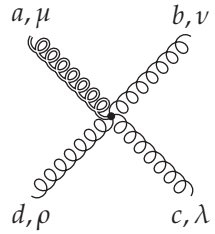


$$-ig^2\Big[f_{abx}f_{xcd}\left(g_{\mu,\lambda}g_{\nu,\rho}-g_{\mu,\rho}g_{\nu,\lambda}\right)+f_{adx}f_{xbc}\left(g_{\mu,\nu}g_{\lambda,\rho}-g_{\mu,\lambda}g_{\nu,\rho}\right)+f_{acx}f_{xbd}\left(g_{\mu,\nu}g_{\lambda,\rho}-g_{\mu,\rho}g_{\nu,\lambda}\right)\Big]$$

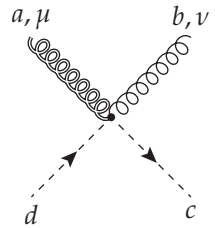


$$-ig^2f_{cax}f_{xbd}g_{\mu\nu}$$

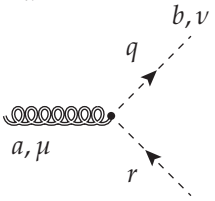


$$-gf_{bac}(r+q)_{\mu}$$

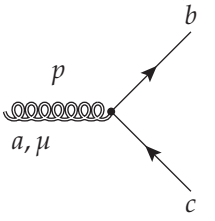


$$-ig\gamma^{\mu}(t^a)^b_c$$

Table 5: Additional Feynman rules for the background field. Note the dependence on $1/\xi$ in the background-gluon-gluon vertex.

computation has been restricted to the Feynman gauge, $\xi_F = 1 - \xi = 0$. An extension to the first power in $\xi_F$ would be considerably slower; the five-loop computation for a general $\xi$ would be impossible without substantial further optimisations of our code. Instead of varying $\xi$, we have checked our computations by verifying the relation $Q_\mu Q_\nu \, \Pi_B^{\mu\nu} = 0$ required by eq. (277). This check took considerably more time than the actual determination of $\beta_4$ due to the increase in tensor rank.

The five-loop diagrams have been calculated on computers with a combined total of more than 500 cores, 80% of which are older and slower by a factor of almost three than the latest Intel Xeon 2.6 GHz workstations. One core of the latter performs a 'raw-speed' Form benchmark, a four-dimensional trace of 14 Dirac matrices, in about 0.02 seconds which corresponds to 50 'form units' (fu) per hour. The total CPU time for the five-loop diagrams was $3.8 \cdot 10^7$ seconds which corresponds to about $2.6 \cdot 10^5$ fu on the computers used. The TForm parallelisation efficiency for single meta diagrams run with 8 or 16 cores was roughly 0.5; the whole calculation of $\beta_4$, distributed 'by hand' over the available machines, finished in three days.

For comparison, the corresponding $R^*$ computation for $\xi_F = 0$ at four loops required about $10^3$ fu, which is roughly the same as for the first computation of the four-loop beta function to order $\xi_F^1$ by a totally different method given in ref. [113]. The computation with the Forcer program at four and fewer loops is much faster, as demonstrated in section 3.11.

The determination of $Z_B$ from the unrenormalised background propagator is performed by imposing, order by order, the finiteness of its renormalised counterpart. The beta function can simply be read off from the $1/\varepsilon$ coefficients of $Z_B$. If the calculation is performed in the Landau gauge, the gauge parameter does not have to be renormalised. In a $k$-th order expansion about the Feynman gauge at five loops, the $L < 5$ loop contributions are needed up to $\xi_F^{5-L}$. The four-loop renormalisation constant for the gauge parameter is not determined in the background field and has to be 'imported'. In the present $k = 0$ case, the terms already specified in ref. [114] would have been sufficient had we not performed the four-loop calculation to all powers of $\xi_F$ anyway.

## 6.4 Results and discussion

Before we present our new results, it may be convenient to recall the beta function (240) up to four loops [23, 24, 113, 114, 119, 120, 122, 210, 211] in terms of the colour factors defined in section 4.1,

$$\beta_0 = \frac{11}{3} C_A - \frac{4}{3} T_F n_f \,, \tag{279}$$

$$\beta_1 = \frac{34}{3} C_A^2 - \frac{20}{3} C_A T_F n_f - 4 C_F T_F n_f \,, \tag{280}$$

$$\beta_2 = \frac{2857}{54} C_A^3 - \frac{1415}{27} C_A^2 T_F n_f - \frac{205}{9} C_F C_A T_F n_f + 2 C_F^2 T_F n_f$$

$$+\ \frac{44}{9}\,C_F\,T_F^2\,n_f^2\ +\ \frac{158}{27}\,C_A\,T_F^2\,n_f^2\ , \tag{281}$$

$$\begin{aligned}
\beta_3\ =\ & C_A^4\left(\frac{150653}{486}-\frac{44}{9}\,\zeta_3\right)+\frac{d_A^{abcd}d_A^{abcd}}{N_A}\left(-\frac{80}{9}+\frac{704}{3}\,\zeta_3\right)\\
&+C_A^3\,T_F\,n_f\left(-\frac{39143}{81}+\frac{136}{3}\,\zeta_3\right)+C_A^2\,C_F\,T_F\,n_f\left(\frac{7073}{243}-\frac{656}{9}\,\zeta_3\right)\\
&+C_A\,C_F^2\,T_F\,n_f\left(-\frac{4204}{27}+\frac{352}{9}\,\zeta_3\right)+\frac{d_F^{abcd}d_A^{abcd}}{N_A}\,n_f\left(\frac{512}{9}-\frac{1664}{3}\,\zeta_3\right)\\
&+46\,C_F^3\,T_F\,n_f\ +C_A^2T_F^2n_f^2\left(\frac{7930}{81}+\frac{224}{9}\,\zeta_3\right)+C_F^2\,T_F^2\,n_f^2\left(\frac{1352}{27}-\frac{704}{9}\,\zeta_3\right)\\
&+C_A\,C_F\,T_F^2\,n_f^2\left(\frac{17152}{243}+\frac{448}{9}\,\zeta_3\right)+\frac{d_F^{abcd}d_F^{abcd}}{N_A}\,n_f^2\left(-\frac{704}{9}+\frac{512}{3}\,\zeta_3\right)\\
&+\frac{424}{243}\,C_A\,T_F^3\,n_f^3\ +\frac{1232}{243}\,C_F\,T_F^3\,n_f^3\ ,
\end{aligned} \tag{282}$$

where $n_f$ is the number of fermion (in QCD, quark) flavours. $\beta_n$ are the same in all MS-like schemes [130, 131], i.e. within the class of renormalisation schemes which differ only by a shift of the scale $\mu$.

Below we will present the results (A) for a generic Yang-Mills theory, (B) for QCD, and (C) for QED.

(A) YANG-MILLS In the same notation and scheme, the five-loop contribution reads

$$\begin{aligned}
\beta_4\ =\ & C_A^5\left(\frac{8296235}{3888}-\frac{1630}{81}\,\zeta_3+\frac{121}{6}\,\zeta_4-\frac{1045}{9}\,\zeta_5\right)\\
&+\frac{d_A^{abcd}d_A^{abcd}}{N_A}\,C_A\left(-\frac{514}{3}+\frac{18716}{3}\,\zeta_3-968\,\zeta_4-\frac{15400}{3}\,\zeta_5\right)\\
&+C_A^4\,T_F\,n_f\left(-\frac{5048959}{972}+\frac{10505}{81}\,\zeta_3-\frac{583}{3}\,\zeta_4+1230\,\zeta_5\right)\\
&+C_A^3\,C_F\,T_F\,n_f\left(\frac{8141995}{1944}+146\,\zeta_3+\frac{902}{3}\,\zeta_4-\frac{8720}{3}\,\zeta_5\right)\\
&+C_A^2\,C_F^2\,T_F\,n_f\left(-\frac{548732}{81}-\frac{50581}{27}\,\zeta_3-\frac{484}{3}\,\zeta_4+\frac{12820}{3}\,\zeta_5\right)\\
&+C_A\,C_F^3\,T_F\,n_f\left(3717+\frac{5696}{3}\,\zeta_3-\frac{7480}{3}\,\zeta_5\right)-C_F^4\,T_F\,n_f\left(\frac{4157}{6}+128\,\zeta_3\right)\\
&+\frac{d_A^{abcd}d_A^{abcd}}{N_A}\,T_F\,n_f\left(\frac{904}{9}-\frac{20752}{9}\,\zeta_3+352\,\zeta_4+\frac{4000}{9}\,\zeta_5\right)\\
&+\frac{d_F^{abcd}d_A^{abcd}}{N_A}\,C_A\,n_f\left(\frac{11312}{9}-\frac{127736}{9}\,\zeta_3+2288\,\zeta_4+\frac{67520}{9}\,\zeta_5\right)
\end{aligned}$$

$$
\begin{aligned}
&+ \frac{d_F^{abcd} d_A^{abcd}}{N_A} C_F\, n_f \left(-320 + \frac{1280}{3}\,\zeta_3 + \frac{6400}{3}\,\zeta_5\right) \\
&+ C_A^3\, T_F^2\, n_f^2 \left(\frac{843067}{486} + \frac{18446}{27}\,\zeta_3 - \frac{104}{3}\,\zeta_4 - \frac{2200}{3}\,\zeta_5\right) \\
&+ C_A^2\, C_F\, T_F^2\, n_f^2 \left(\frac{5701}{162} + \frac{26452}{27}\,\zeta_3 - \frac{944}{3}\,\zeta_4 + \frac{1600}{3}\,\zeta_5\right) \\
&+ C_F^2\, C_A\, T_F^2\, n_f^2 \left(\frac{31583}{18} - \frac{28628}{27}\,\zeta_3 + \frac{1144}{3}\,\zeta_4 - \frac{4400}{3}\,\zeta_5\right) \\
&+ C_F^3\, T_F^2\, n_f^2 \left(-\frac{5018}{9} - \frac{2144}{3}\,\zeta_3 + \frac{4640}{3}\,\zeta_5\right) \\
&+ \frac{d_F^{abcd} d_A^{abcd}}{N_A} T_F\, n_f^2 \left(-\frac{3680}{9} + \frac{40160}{9}\,\zeta_3 - 832\,\zeta_4 - \frac{1280}{9}\,\zeta_5\right) \\
&+ \frac{d_F^{abcd} d_F^{abcd}}{N_A} C_A\, n_f^2 \left(-\frac{7184}{3} + \frac{40336}{9}\,\zeta_3 - 704\,\zeta_4 + \frac{2240}{9}\,\zeta_5\right) \\
&+ \frac{d_F^{abcd} d_F^{abcd}}{N_A} C_F\, n_f^2 \left(\frac{4160}{3} + \frac{5120}{3}\,\zeta_3 - \frac{12800}{3}\,\zeta_5\right) \\
&+ C_A^2\, T_F^3\, n_f^3 \left(-\frac{2077}{27} - \frac{9736}{81}\,\zeta_3 + \frac{112}{3}\,\zeta_4 + \frac{320}{9}\,\zeta_5\right) \\
&+ C_A\, C_F\, T_F^3\, n_f^3 \left(-\frac{736}{81} - \frac{5680}{27}\,\zeta_3 + \frac{224}{3}\,\zeta_4\right) \\
&+ C_F^2\, T_F^3\, n_f^3 \left(-\frac{9922}{81} + \frac{7616}{27}\,\zeta_3 - \frac{352}{3}\,\zeta_4\right) \\
&+ \frac{d_F^{abcd} d_F^{abcd}}{N_A} T_F\, n_f^3 \left(\frac{3520}{9} - \frac{2624}{3}\,\zeta_3 + 256\,\zeta_4 + \frac{1280}{3}\,\zeta_5\right) \\
&+ C_A\, T_F^4\, n_f^4 \left(\frac{916}{243} - \frac{640}{81}\,\zeta_3\right) - C_F\, T_F^4\, n_f^4 \left(\frac{856}{243} + \frac{128}{27}\,\zeta_3\right) \,. \qquad (283)
\end{aligned}
$$

$\zeta$ denotes the Riemann zeta function with $\zeta_3 \cong 1.202056903$, $\zeta_4 = \pi^4/90 \cong 1.08232323$ and $\zeta_5 \cong 1.036927755$. As expected from the lower-order and QED results, higher values of the zeta function do not occur despite their occurrence in the results for individual diagrams; for further discussions see ref. [105, 204, 213].

(B) QCD Inserting the group factors of $SU(3)$ as given in eq. (62) leads to the QCD results

$$
\begin{aligned}
\beta_0 &= 11 - \frac{2}{3}\,n_f \,, \qquad \beta_1 = 102 - \frac{38}{3}\,n_f \,, \\
\beta_2 &= \frac{2857}{2} - \frac{5033}{18}\,n_f + \frac{325}{54}\,n_f^2 \,,
\end{aligned}
$$

$$\beta_3 = \frac{149753}{6} + 3564\,\zeta_3 + n_f\left(-\frac{1078361}{162} - \frac{6508}{27}\,\zeta_3\right) + n_f^2\left(\frac{50065}{162} + \frac{6472}{81}\,\zeta_3\right) + \frac{1093}{729}\,n_f^3 \tag{284}$$

and

$$\begin{aligned}\beta_4 = {} & \frac{8157455}{16} + \frac{621885}{2}\,\zeta_3 - \frac{88209}{2}\,\zeta_4 - 288090\,\zeta_5 \\ & + n_f\left(-\frac{336460813}{1944} - \frac{4811164}{81}\,\zeta_3 + \frac{33935}{6}\,\zeta_4 + \frac{1358995}{27}\,\zeta_5\right) \\ & + n_f^2\left(\frac{25960913}{1944} + \frac{698531}{81}\,\zeta_3 - \frac{10526}{9}\,\zeta_4 - \frac{381760}{81}\,\zeta_5\right) \\ & + n_f^3\left(-\frac{630559}{5832} - \frac{48722}{243}\,\zeta_3 + \frac{1618}{27}\,\zeta_4 + \frac{460}{9}\,\zeta_5\right) + n_f^4\left(\frac{1205}{2916} - \frac{152}{81}\,\zeta_3\right)\end{aligned} \tag{285}$$

In truncated numerical form $\beta_3$ and $\beta_4$ are given by

$$\beta_3 \cong 29242.964 - 6946.2896\,n_f + 405.08904\,n_f^2 + 1.499314\,n_f^3\,, \tag{286}$$

$$\beta_4 \cong 537147.67 - 186161.95\,n_f + 17567.758\,n_f^2 - 231.2777\,n_f^3 - 1.842474\,n_f^4 \tag{287}$$

In contrast to $\beta_0$, $\beta_1$, and $\beta_2$, which change sign at about $n_f = 16.5$, 8.05, and 5.84 respectively, $\beta_3$ and $\beta_4$ are positive (except at very large $n_f$ for $\beta_4$), but have a (local) minimum at $n_f \simeq 8.20$ and $n_f \simeq 6.07$.

(c) QED The corresponding analytical result for QED, in the same renormalisation scheme(s) but defined without the overall minus sign in eq. (240) is given by

$$\beta_0 = \frac{4}{3}\,n_f\,, \quad \beta_1 = 4\,n_f\,, \quad \beta_2 = -2\,n_f - \frac{44}{9}\,n_f^2\,,$$

$$\beta_3 = -46\,n_f + n_f^2\left(\frac{760}{27} - \frac{832}{9}\,\zeta_3\right) - \frac{1232}{243}\,n_f^3 \tag{288}$$

and

$$\begin{aligned}\beta_4 = {} & n_f\left(\frac{4157}{6} + 128\,\zeta_3\right) + n_f^2\left(-\frac{7462}{9} - 992\,\zeta_3 + 2720\,\zeta_5\right) \\ & + n_f^3\left(-\frac{21758}{81} + \frac{16000}{27}\,\zeta_3 - \frac{416}{3}\,\zeta_4 - \frac{1280}{3}\,\zeta_5\right) + n_f^4\left(\frac{856}{243} + \frac{128}{27}\,\zeta_3\right)\end{aligned} \tag{289}$$

The (corresponding parts of the) results (283), (285) and (289) are in complete agreement with the findings of refs. [40, 128, 213, 214]. Consequently, eq. (289) also agrees with the result for QED at $n_f = 1$, which was obtained in ref. [44] somewhat earlier than the general result [213].

In the following sections we will analyse three properties of the beta function. First, we study the $n_f$-dependence in section 6.4.1. Then, we analyse the $N$-dependence in section 6.4.2. Finally, we study the cumulative effects of the QCD beta function corrections in section 6.4.3

### 6.4.1 *Analysis of $n_f$-dependence in QCD*

As already noted in ref. [40], the five-loop *QCD* coefficient of the beta function is rather small [recall that we use a convenient but very small expansion parameter in eq. (240)]. Indeed, for the physically relevant values of $n_f$ the expansion in powers of $a_s$ reads

$$\begin{aligned}
\widetilde{\beta}(a_s, n_f=3) &= 1 + 0.565884\, a_s + 0.453014\, a_s^2 + 0.676967\, a_s^3 + 0.580928\, a_s^4 \,, \\
\widetilde{\beta}(a_s, n_f=4) &= 1 + 0.490197\, a_s + 0.308790\, a_s^2 + 0.485901\, a_s^3 + 0.280601\, a_s^4 \,, \\
\widetilde{\beta}(a_s, n_f=5) &= 1 + 0.401347\, a_s + 0.149427\, a_s^2 + 0.317223\, a_s^3 + 0.080921\, a_s^4 \,, \\
\widetilde{\beta}(a_s, n_f=6) &= 1 + 0.295573\, a_s - 0.029401\, a_s^2 + 0.177980\, a_s^3 + 0.001555\, a_s^4 \,,
\end{aligned} \tag{290}$$

where $\widetilde{\beta} \equiv -\beta(a_s)/(a_s^2\beta_0)$ has been re-expanded in powers of $a_s = 4\pi\, a_s$. Clearly there is no sign so far of a possible divergence of the perturbation series for this quantity.

In order to further illustrate the $n_f$-dependent convergence (or the lack thereof) of the beta function of QCD, we introduce the quantity

$$\widehat{a}_s^{(n)}(n_f) \;=\; 4\pi \left| \frac{\beta_{n-1}(n_f)}{4\,\beta_n(n_f)} \right| \,. \tag{291}$$

Recalling the normalisation (240) of our expansion parameter, $\widehat{a}_s^{(n)}(n_f)$ represents the value of $a_s$ for which the $n$-th order correction is $1/4$ of that of the previous order. Therefore, $a_s \lesssim \widehat{a}_s^{(n)}(n_f)$ defines (somewhat arbitrarily due to the choice of a factor of $1/4$) a region of fast convergence of $\beta(a_s, n_f)$. Obviously, the absolute size of the $n$-th and $(n-1)$-th order effects are equal for $a_s = 4\,\widehat{a}^{(n)}(n_f)$. Thus the quantity (291) also indicates where the expansion appears not to be reliable anymore, $a_s \gtrsim 4\,\widehat{a}_s^{(n)}(n_f)$, for a given value of $n_f$ that is not too close to zeros or minima of the coefficients $\beta_{n-1}$ and $\beta_n$.

### 6.4.2 *Analysis of N-dependence in SU(N)*

It is interesting to briefly study the $N$-dependence of the convergence behaviour for the case of SU($N$) gauge theories. For our brief illustration we confine ourselves to pure Yang-Mills theory, $n_f = 0$, and consider

$$\widehat{a}_{\rm YM}^{(n)}(N) \;=\; 4\pi\, N \left| \frac{\beta_{n-1}(N)}{4\,\beta_n(N)} \right| \,, \tag{292}$$

where the factor $N$ compensates the leading large-$N$ dependence $N^{n+1}$ of $\beta_n$, i.e., the parameter that needs to be small in $SU(N)$ Yang-Mills theory is not $a_{\rm YM}$ but $N a_{\rm YM}$.

The quantities (291) and (292) are displayed in the left and right panel of figure 33, respectively. The behaviour of $\widehat{a}_{\rm s}^{(n)}$ at the upper end of the $n_f$ range shown in the figure is affected by the zeros and minima of the coefficients $\beta_n > 0$ mentioned below eq. (287). The $N$-dependence of $\widehat{a}_{\rm YM}$ for pure Yang-Mills theory, where only terms with $N^{n+1}$ and $N^{n-1}$ enter $\beta_n$ (the latter only at $n \geq 4$ via $d_A^{abcd} d_A^{abcd}/N_A$, cf. eq. (62) above), is rather weak. With only the curves up to four loops, one might be tempted to draw conclusions from the shrinking of the 'stable' $a_{\rm s}$ region from NLO to N$^2$LO and from N$^2$LO to N$^3$LO that are not supported by the N$^4$LO (five-loop) results of ref. [40] and the present section.

### 6.4.3 *Cumulative effects of the QCD beta function corrections*

Finally, we briefly illustrate the cumulative effect of the orders up to N$^4$LO on the beta function of QCD and the scale dependence of the strong coupling constant $a_{\rm s}$ in figure 34. For this illustration we set $n_f = 4$ and choose, in order to only show the differences caused by the running of the coupling, an order-independent value of $a_{\rm s} = 0.2$ at $\mu^2 = 40\,\text{GeV}^2$. A realistic order dependence of $a_{\rm s}$ at this scale, as determined from the scaling violations in DIS, would be 0.208, 0.201, 0.200, and 0.200 at NLO, N$^2$LO, N$^3$LO, and N$^4$LO, respectively [98].

Adding the N$^4$LO contributions changes the beta function by less than 1% at $a_{\rm s} = 0.47$ for $n_f = 4$ and at $a_{\rm s} = 0.39$ for $n_f = 3$; the corresponding values at N$^3$LO are 0.29 and 0.26. The N$^4$LO effect on the values of $a_{\rm s}$ as shown in figure 34 are as small as 0.08% (0.4%) at $\mu^2 = 3\,\text{GeV}^2$ (1 GeV$^2$); the corresponding N$^3$LO corrections are 0.5% (2%). Of course, these results do not preclude sizeable purely non-perturbative corrections, but it appears that the perturbative running of $a_{\rm s}$ is now fully under control for all practical purposes.

## 6.5 QCD BETA FUNCTION IN THE MINIMOM SCHEME

Unlike the $\overline{\rm MS}$ scheme, momentum subtraction schemes are defined in a regularisation-independent way. In these schemes, the field renormalisations are performed such

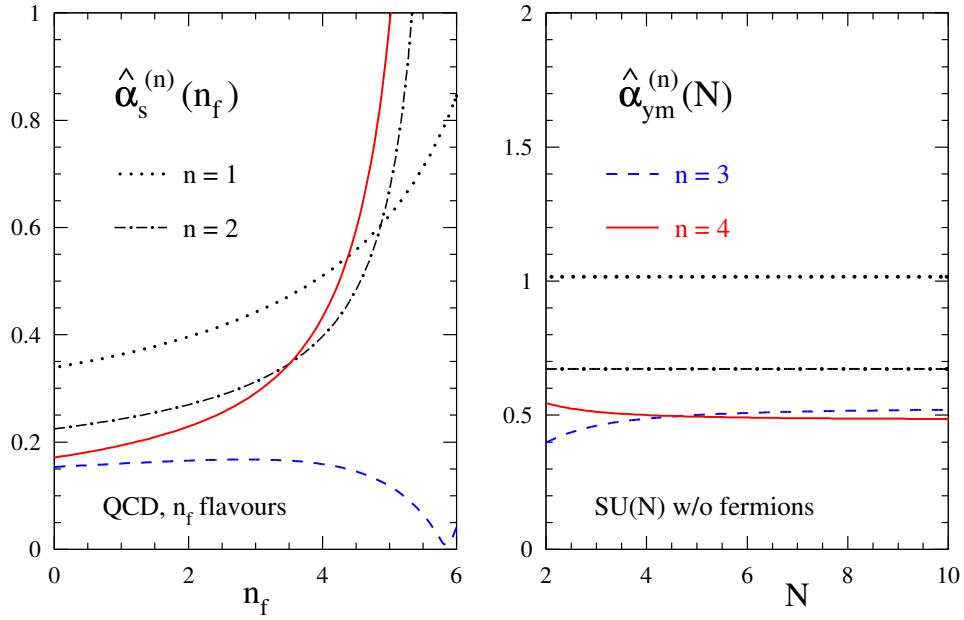


Figure 33: The values (291) and (292) of the coupling constants of QCD (left) and pure SU($N$) Yang-Mills theory (right) for which the absolute size of the $\mathrm{N}^n\mathrm{LO}$ contribution to the beta function is a quarter of that of the $\mathrm{N}^{n-1}\mathrm{LO}$ term for $n = 1, 2, 3$ (dashed curves) and 4 (solid curves).

that finite radiative corrections on propagators are absorbed as well as divergences and hence they coincide with their tree-level values at the renormalisation point. Then one of (or an arbitrary linear combination of) the vertex functions is normalised to its tree-level value and the other vertices are fixed via the Slavnov-Taylor identities. Common choices for the subtraction point of the vertex are a symmetric point (referred as MOM schemes) and an asymmetric point where one of the momenta is nullified, sometimes referred as $\widetilde{\mathrm{MOM}}$ schemes. The latter choice corresponds to our result for the vertex functions, given in section 4.2. Indeed, ref. [139] derived four-loop beta functions in four particular $\widetilde{\mathrm{MOM}}$ schemes from that in the $\overline{\mathrm{MS}}$ scheme by computing conversion factors via finite parts of two- and three-point functions in the $\overline{\mathrm{MS}}$ scheme.

As an example application, we provide the five-loop beta function in the minimal momentum subtraction (MiniMOM) scheme introduced in ref. [153], thus extending previous results [153, 217] by one order in the coupling constant. This scheme, see the preceding references for a detailed discussion, is more convenient than $\overline{\mathrm{MS}}$ for extending analyses of the strong coupling constant and its scale dependence into the non-perturbative regime, e.g., via lattice QCD; for a recent analysis see ref. [218]. In the perturbative regime the MiniMOM scheme provides an alternative to $\overline{\mathrm{MS}}$ for studying the behaviour and truncation uncertainty of the perturbation series for

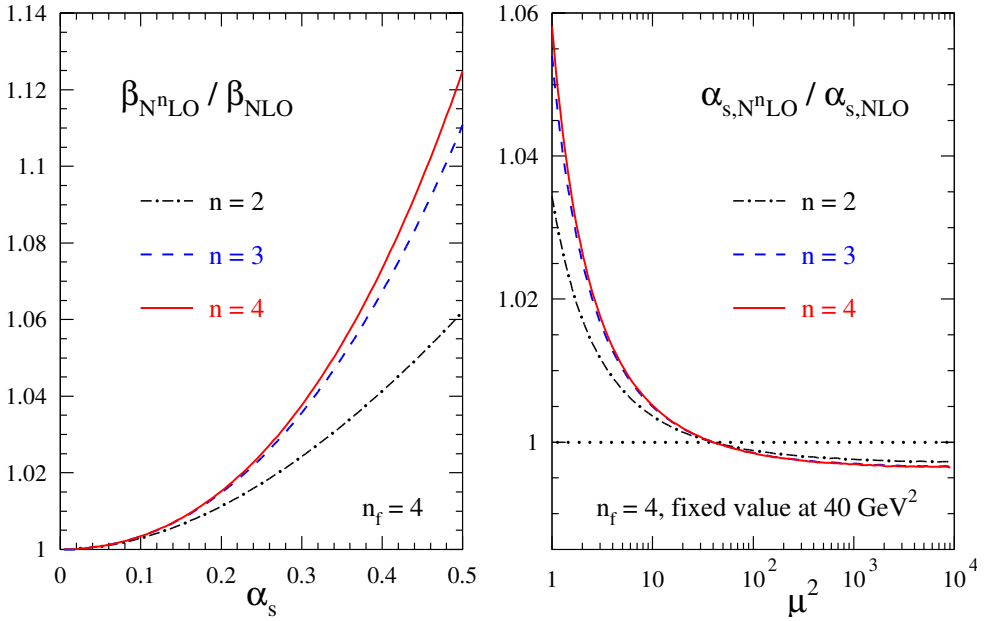


Figure 34: Left panel: The total N$^2$LO, N$^3$LO and N$^4$LO results for the beta function of QCD for four flavours, normalised to the NLO approximation. Right panel: The resulting scale dependence of $\alpha_s$ for a value of 0.2 at 40 GeV$^2$, also normalised to the NLO result in order to show the small higher-order effects more clearly, for the scale range 1 GeV$^2 \leq \mu^2 \leq 10^4$ GeV$^2$.

benchmark quantities such as the $R$-ratio in $e^+e^-$ annihilation and the Higgs-boson decay to gluons, see refs. [219, 220].

In the MiniMOM scheme [153], the self-energies are completely absorbed into the field renormalisation constants at the subtraction point $q^2 = -\mu^2$:

$$1 + \Pi^{\mathrm{MM}}(-\mu^2) = Z_3^{\mathrm{MM}}\left[1 + \Pi^B(-\mu^2)\right] = 1, \tag{293}$$

$$1 + \tilde{\Pi}^{\mathrm{MM}}(-\mu^2) = \tilde{Z}_3^{\mathrm{MM}}\left[1 + \tilde{\Pi}^B(-\mu^2)\right] = 1, \tag{294}$$

$$1 + \Sigma_V^{\mathrm{MM}}(-\mu^2) = Z_2^{\mathrm{MM}}\left[1 + \Sigma_V^B(-\mu^2)\right] = 1. \tag{295}$$

Here the superscript "MM" indicates a quantity in the MiniMOM scheme. In addition, motivated by the non-renormalisation of the ghost-gluon vertex in the Landau gauge [221], the vertex renormalisation constant for this vertex is chosen the same as that in $\overline{\mathrm{MS}}$,

$$\tilde{Z}_1^{\mathrm{MM}} = \tilde{Z}_1^{\overline{\mathrm{MS}}}, \tag{296}$$

which is equal to one in the Landau gauge.

The above renormalisation conditions lead to the following relations for the coupling constant and gauge parameter in the two schemes:

$$a^{\rm MM}(\mu^2) \;=\; a^{\overline{\rm MS}}(\mu^2)\,\frac{1}{\left[1+\Pi^{\overline{\rm MS}}(-\mu^2)\right]\left[1+\tilde{\Pi}^{\overline{\rm MS}}(-\mu^2)\right]^2}\,, \tag{297}$$

$$\xi^{\overline{\rm MS}}(\mu^2) \;=\; \xi^{\rm MM}(\mu^2)\,\frac{1}{1+\Pi^{\overline{\rm MS}}(-\mu^2)}\,. \tag{298}$$

eq. (297) allows one to convert a value of $\alpha_s^{\overline{\rm MS}}$ to $\alpha_s^{\rm MM}$. For example, $\alpha_s^{\overline{\rm MS}}(M_Z^2) = 0.118$ leads to $\alpha_s^{\rm MM}(M_Z^2) = 1.096\,\alpha_s^{\overline{\rm MS}}(M_Z^2)$ for QCD in the Landau gauge with $n_f = 5$ quark flavours. The general expansion of eq. (297) is given in [2].

The scale dependence of the coupling constant in eq. (297) in this scheme is given by

$$\beta^{\rm MM} \;=\; \mu^2\frac{da^{\rm MM}}{d\mu^2} \;=\; \frac{\partial a^{\rm MM}}{\partial a^{\overline{\rm MS}}}\beta^{\overline{\rm MS}} \;+\; \frac{\partial a^{\rm MM}}{\partial \xi^{\overline{\rm MS}}}\gamma_3^{\overline{\rm MS}}\xi^{\overline{\rm MS}}, \tag{299}$$

where we have used the beta function and gluon field anomalous dimension in $\overline{\rm MS}$,

$$\beta^{\overline{\rm MS}} \;=\; \mu^2\frac{da^{\overline{\rm MS}}}{d\mu^2}\,, \tag{300}$$

$$\gamma_3^{\overline{\rm MS}}\xi^{\overline{\rm MS}} \;=\; \mu^2\frac{d\xi^{\overline{\rm MS}}}{d\mu^2}\,. \tag{301}$$

Note that the right-hand side of eq. (297), and hence that of eq. (299), is naturally given in terms of $a^{\overline{\rm MS}}$ and $\xi^{\overline{\rm MS}}$. One has to convert them into $a^{\rm MM}$ and $\xi^{\rm MM}$ by inverting the series of eq. (297) and by using eq. (298).[2]

Having results for the four-loop self-energies in the $\overline{\rm MS}$ scheme at hand (see section 4.2), one can obtain the five-loop beta function in the MiniMOM scheme from the five-loop beta function [4, 40] and the four-loop gluon field anomalous dimension in the $\overline{\rm MS}$ scheme. The result for SU(3) in the Landau gauge ($\xi^{\rm MM} = 0$) reads

$$\beta^{\rm MM} \;=\; -\sum_{l=0}^{4}\left(a^{\rm MM}\right)^{l+2}\beta_l^{\rm MM} \;+\; \mathcal{O}\Big(\left(a^{\rm MM}\right)^7\Big), \tag{302}$$

with

$$\beta_0^{\rm MM} = 11 - \frac{2}{3}n_f,$$

$$\beta_1^{\rm MM} = 102 - \frac{38}{3}n_f,$$

2 In ref. [153], the results are presented in $\xi^{\overline{\rm MS}}$ instead of $\xi^{\rm MM}$. In contrast, in ref. [217] the conversion from $\xi^{\overline{\rm MS}}$ to $\xi^{\rm MM}$ was performed. The results become the same in the Landau gauge $\xi^{\overline{\rm MS}} = \xi^{\rm MM} = 0$. The same is true for the "$\widetilde{\rm MOM}$h" scheme of ref. [139].

$$
\begin{aligned}
\beta_2^{\rm MM} &= \left(\frac{28965}{8} - \frac{3861}{8}\zeta_3\right) + n_f\left(-\frac{7715}{12} + \frac{175}{12}\zeta_3\right) + {n_f}^2\left(\frac{989}{54} + \frac{8}{9}\zeta_3\right),\\
\beta_3^{\rm MM} &= \left(\frac{1380469}{8} - \frac{625317}{16}\zeta_3 - \frac{772695}{32}\zeta_5\right) + n_f\left(-\frac{970819}{24} + \frac{516881}{72}\zeta_3\right.\\
&\quad \left. + \frac{1027375}{144}\zeta_5\right) + {n_f}^2\left(\frac{736541}{324} - \frac{6547}{27}\zeta_3 - \frac{9280}{27}\zeta_5\right) + {n_f}^3\left(-\frac{800}{27} + \frac{16}{9}\zeta_3\right),\\
\beta_4^{\rm MM} &= \left(\frac{3248220045}{256} - \frac{1064190195}{512}\zeta_3 - \frac{4922799165}{512}\zeta_5 - \frac{7696161}{64}{\zeta_3}^2\right.\\
&\quad \left. + \frac{21619456551}{4096}\zeta_7\right) + n_f\left(-\frac{115659378547}{31104} + \frac{10327103555}{20736}\zeta_3 + \frac{18219328375}{6912}\zeta_5\right.\\
&\quad \left. + \frac{82869}{32}{\zeta_3}^2 - \frac{24870449471}{18432}\zeta_7\right) + {n_f}^2\left(\frac{833934985}{2592} - \frac{13019053}{1296}\zeta_3 - \frac{65264845}{324}\zeta_5\right.\\
&\quad \left. + \frac{59531}{36}{\zeta_3}^2 + \frac{26952037}{432}\zeta_7\right) + {n_f}^3\left(-\frac{3249767}{324} - \frac{129869}{162}\zeta_3 + \frac{299875}{54}\zeta_5\right.\\
&\quad \left. - \frac{2240}{27}{\zeta_3}^2\right) + {n_f}^4\left(\frac{2617}{27} + \frac{304}{27}\zeta_3 - \frac{1760}{27}\zeta_5\right). \qquad (303)
\end{aligned}
$$

Due to its length, we do not show the result with a generic group and arbitrary covariant linear gauge here. Instead, we refer the readers to ref. [2]. Our result agrees with the result given in ref. [217] up to four loops. As is well known, the first coefficient $\beta_0^{\rm MM}$ is scheme independent. The next coefficient $\beta_1^{\rm MM}$ has a gauge dependence and the universal value is obtained only in the Landau gauge. The last coefficient $\beta_4^{\rm MM}$ is the new result. In the $\overline{\rm MS}$ scheme, some of higher values of the zeta function (e.g., $\zeta_3^2$, $\zeta_6$ and $\zeta_7$ at five loops) do not occur, for a discussion of this issue see refs. [105, 203, 204]. In contrast, one cannot expect their absence in the MiniMOM scheme. Indeed eq. (303) includes terms with $\zeta_3^2$ and $\zeta_7$, and for $\xi^{\rm MM} \neq 0$ also $\zeta_6$ occurs.

The numerical values of the above beta function for three to five quark flavours are

$$
\begin{aligned}
\tilde{\beta}^{\rm MM}(n_f = 3) &= 1 + 0.5658842421\alpha_{\rm s}^{\rm MM} + 0.9419859046(\alpha_{\rm s}^{\rm MM})^2\\
&\quad + 2.304494526(\alpha_{\rm s}^{\rm MM})^3 + 6.647485913(\alpha_{\rm s}^{\rm MM})^4,\\
\tilde{\beta}^{\rm MM}(n_f = 4) &= 1 + 0.4901972247\alpha_{\rm s}^{\rm MM} + 0.6452147391(\alpha_{\rm s}^{\rm MM})^2\\
&\quad + 1.638457168(\alpha_{\rm s}^{\rm MM})^3 + 3.466865543(\alpha_{\rm s}^{\rm MM})^4,\\
\tilde{\beta}^{\rm MM}(n_f = 5) &= 1 + 0.4013472477\alpha_{\rm s}^{\rm MM} + 0.3288519562(\alpha_{\rm s}^{\rm MM})^2\\
&\quad + 1.026892491(\alpha_{\rm s}^{\rm MM})^3 + 0.8417657296(\alpha_{\rm s}^{\rm MM})^4,
\end{aligned} \qquad (304)
$$

where $\tilde{\beta} \equiv \beta(a)/(-\beta_0 a^2)$ has been re-expanded in powers of $\alpha_s = 4\pi a$. These values may be compared with those in the $\overline{\text{MS}}$ scheme [4, 40] reading

$$\begin{aligned}
\tilde{\beta}^{\overline{\text{MS}}}(n_f = 3) &= 1 + 0.5658842421\alpha_s^{\overline{\text{MS}}} + 0.4530135791(\alpha_s^{\overline{\text{MS}}})^2 \\
&\quad + 0.6769674420(\alpha_s^{\overline{\text{MS}}})^3 + 0.5809276379(\alpha_s^{\overline{\text{MS}}})^4, \\
\tilde{\beta}^{\overline{\text{MS}}}(n_f = 4) &= 1 + 0.4901972247\alpha_s^{\overline{\text{MS}}} + 0.3087903795(\alpha_s^{\overline{\text{MS}}})^2 \\
&\quad + 0.4859007965(\alpha_s^{\overline{\text{MS}}})^3 + 0.2806008338(\alpha_s^{\overline{\text{MS}}})^4, \\
\tilde{\beta}^{\overline{\text{MS}}}(n_f = 5) &= 1 + 0.4013472477\alpha_s^{\overline{\text{MS}}} + 0.1494273313(\alpha_s^{\overline{\text{MS}}})^2 \\
&\quad + 0.3172233974(\alpha_s^{\overline{\text{MS}}})^3 + 0.08092104151(\alpha_s^{\overline{\text{MS}}})^4.
\end{aligned} \tag{305}$$

Obviously, the MiniMOM coefficients in eqs. (304) are (much) larger than their $\overline{\text{MS}}$ counterparts in eqs. (305) starting from the second order; moreover, they exhibit a definite growth with the order that is absent in the $\overline{\text{MS}}$ case. One may expect that this behaviour, and the larger value of $\alpha_s^{\text{MM}}$, is more than compensated by smaller expansion coefficients for observables, leading to a better overall convergence in MOM-like schemes. However, this issue has been studied up to four loops in some detail for the $R$-ratio in electron-positron annihilation, without arriving at such a clear-cut conclusion [219].

## 6.6 CHAPTER CONCLUSIONS

We have presented five methods to improve the performance of the $R^*$-operation when applied to five-loop diagrams: (1) extraction of propagator insertions, (2) delayed Feynman rule substitution, (3) efficient rules to make diagrams logarithmic, (4) a canonical form algorithm suitable for Feynman diagrams, and (5) an efficient tensor reduction routine.

Next, we have defined the background field, which makes it convenient to extract the five-loop beta function. Using the background field propagator, we have computed the five-loop (next-to-next-to-next-to-next-to-leading order, N$^4$LO) coefficient $\beta_4$ of the renormalisation-group beta function in MS-like schemes for Yang-Mills theory with a simple compact Lie group and one set of $n_f$ spin-1/2 fermions. This computation confirms and extends the QCD and QED results first obtained, respectively, in ref. [40] – where also some direct phenomenological applications to $\alpha_s$ determinations and Higgs-boson decay have already been discussed – and ref. [213]. It also agrees with the high-$n_f$ partial results of refs. [128, 214]. We have verified our result and method by confirming the transversality of the background field propagator.

We have illustrated the size of the resulting N$^4$LO corrections to the scale dependence of the coupling constant for $\alpha_s$-values relevant to $\overline{\text{MS}}$, the default scheme for higher-order calculations and analyses in perturbative QCD. For physical values of $n_f$, the N$^4$LO corrections to the beta function are much smaller than the N$^3$LO

contributions and amount to 1% or less, even for $\alpha_s$-values as large as 0.4. More generally, there is no evidence of any increase of the coefficients indicative of a non-convergent perturbative expansion for the beta functions of QCD and SU($N$) gauge theories.

The computations make extensive use of Forcer, as described in chapter 3, and the $R^*$-operation described in chapter 5.

Using the four-loop propagators and vertices computed in chapter 4, we have determined the five-loop beta function in the MiniMOM scheme of ref. [153], i.e., we have extended the result of refs. [153, 217] by one order in the coupling constant $\alpha_s$.

A Form file with our result for the coefficient $\beta_4$ and its lower-order counterparts can be obtained from the preprint server arXiv in the source of [4]. The beta function in the MiniMOM scheme with full gauge dependence and for generic colour group is provided as an ancillary file on arXiv of [2].

### 6.6.1 *Findings and main conclusion*

The main contribution of this chapter is the computation of the five-loop beta function for Yang-Mills theory with fermions. For this computation both the Forcer program (the answer to **RQ2**) and the new generalised $R^*$ method with its computer code (the answer to **RQ3**) were critical. Our computation took six days on a 32-core machine. The QCD result we verified from [40] took 1.5 years on 20 workstations with 8 cores.

Our main conclusion therefore reads as follows: we have succeeded to compute the five-loop beta function in six days, verifying the existing QCD result and extending it to a generic Yang-Mills theory with fermions.

### 6.6.2 *Future work*

As of this moment we envisage two future projects. First, we have seen that the beta function in the MiniMOM scheme appears to have a higher-order structure which is quite different from that in the $\overline{\text{MS}}$ scheme, thus inviting further studies especially for the physical case of QCD in four dimensions.

Second, the beta function could be extended to six loops. However, this will be a tremendous challenge for at least three reasons: (1) a five-loop Forcer equivalent has to be built, (2) substituting the Feynman rules will create billions of terms, and (3) the number of counterterms will become enormous.